ORNL/SPR-2019/1067

Synthesis and Characterization of UO_2 Feedstocks Containing Controlled Dopants

Nuclear Technology Research and Development

Prepared for
US Department of Energy
Advanced Fuel Campaign
S. C. Finkeldei,
R. D. Hunt, J. O. Kiggans
C. A. Hobbs, B. D. Eckhart,
J. W. McMurray, D. R. Brown,
G. Helmreich, K. A. Terrani
A. T. Nelson
Oak Ridge National Laboratory
January 2019
M3FT-19OR020201075

SUMMARY

Within the Advanced Fuels Campaign, the Oak Ridge National Laboratory is looking into the fabrication of high-performance UO_2 fuel candidates. The aim of this study was to develop a suitable fabrication avenue to synthesize UO_2 feedstock with controlled dopants to enhance UO_2 grain growth within these fuel candidates. Enlarged UO_2 grains in a nuclear fuel pellet are expected to slow down fission gas diffusion, which would be a preferred property for a high-performance fuel compared to fission gas diffusion in standard UO_2. The unique fabrication processes for microspherical feedstocks via the internal gelation approach at the Oak Ridge National Laboratory have been developed further to enable the dopant uptake within the UO_2 microspheres. Mn and Cr were added via infiltration and/or addition of the dopant to the starting broth of an internal gelation experiment. The dopants were added in various amounts (ppm) into UO_2. Even though large amounts of these dopants volatized during sintering, scanning electron microscopy images of the microstructure revealed large UO_2 grains of up to 80 μm for the pellets that were prepared from doped microspherical feedstocks.

INTENTIONALLY BLANK

CONTENTS

FIGURES

TABLES

ACRONYMS

ADUN	acid deficient uranyl nitrate
AFC	Advanced Fuels Campaign
HFIR	High Flux Isotope Reactor
HMTA	hexamethylenetetramine
ICP-MS	inductively coupled plasma mass spectrometry
ORNL	Oak Ridge National Laboratory
PCI	pellet-cladding interaction
ppm	parts per million
SEM	scanning electron microscopy
SGMP	sol-gel microsphere pelletization
TCE	trichloroethylene
TD	theoretical density
TGA	thermogravimetric analysis
XCT	x-ray computed tomography
XRD	x-ray diffraction

ACKNOWLEDGMENTS

This work was supported by the US Department of Energy Office of Nuclear Energy (DOE-NE) Advanced Fuels Campaign (AFC). The authors thank Tamara Keever for conducting the inductively coupled plasma mass spectrometry (ICP-MS) analysis.

SYNTHESIS AND CHARACTERIZATION OF UO_2 FEEDSTOCKS CONTAINING CONTROLLED DOPANTS

1. INTRODUCTION

The Advanced Fuels Campaign (AFC) is seeking accident-tolerant fuels (ATF) with properties superior to those found in standard UO_2. Because UO_2 is still the most commonly used fuel for energy production in nuclear power plants, this work focuses on the development and characterization of high-performance UO_2-based fuels with dopants. Engineering of the fuel's microstructure is a key objective in the design of such high-performance UO_2 fuel candidates. This type of engineering is typically approached by adding dopants or larger quantities of secondary inert phases. The latter approach was described in an earlier report [1]. Dopants consist of secondary cations introduced through either wet or dry additions to the UO_2 feedstock during processing steps. They are added at hundred- to thousand-weight parts per million (ppm) levels. This is typically either below or slightly above the solubility of the transition metal in the UO_2 lattice. This causes the secondary cations to either reside on uranium sites or to precipitate out as secondary phases at very small volume fractions. The goal of this approach is to either grow grain sizes and/or alter the mechanical properties of UO_2 of nominal purity. Larger grains have the effect of extending the time it takes for fission products to reach a grain boundary, where they have a quicker escape route. Therefore, fuel with enlarged grains is expected to lead to a slower fission gas release. The addition of Cr_2O_3 has been found to achieve this goal while simultaneously lowering the fracture strength of UO_2. This exasperates cracking of the fuel pellet, limiting its ability to exert force on the cladding and thereby reducing pellet-cladding interaction (PCI). A recent computational study by Cooper et al. [2] proposed Mn to be a highly suitable dopant element to promote grain growth in UO_2, besides already known dopants such as e.g. Cr_2O_3 and Al_2O_3 [3][4][5]. Cooper et al. [2] ascribe the enhanced grain growth to the higher concentration of uranium vacancies caused by incorporation of the dopants. There is currently no experimental evidence in the open literature for the computational prediction of Mn as sole dopant in UO_2 to result in enhanced UO_2 grain growth.

In the present work, Cr and Mn were chosen as dopant elements to promote grain growth in UO_2. In contrast to most approaches presented in the open literature for Cr doped UO_2 fuel candidates [3] [4] [5], efforts at the Oak Ridge National Laboratory (ORNL) were to fabricate a microspherical precursor that is synthesized via an internal sol-gel approach. Kang et al. [6] reported enhanced grain growth via the addition of a combined MnO-Al_2O_3 additive to UO_2 achieved via a solid-state reaction route. In contrast to the Cr-doped feedstocks, the authors find no experimental evidence for enhanced grain growth in UO_2 due to the sole addition of Mn. Once these potentially advanced fuel candidates are fabricated and thoroughly characterized, irradiation will occur in ORNL's MiniFuel irradiation setup. This will allow for post-irradiation examination to gain an understanding of the fuel candidates' response to irradiation and to evaluate their suitability for in-reactor application with a focus on fission gas diffusion.

2. FABRICATION OF UO_3 FEEDSTOCKS

UO_3 microspheres were fabricated via an established internal gelation process at ORNL [7]. A solution of the desired amounts of acid-deficient uranyl nitrate (ADUN) and hexamethylenetetramine (HMTA)/urea was chilled in an ice bath and mixed cold. The chilled solution was transferred into a chilled broth pot in the sol-gel set-up and pumped into the heated gelation column, where the gelation of the dispersed droplets took place. After aging in the hot gelation medium, the spheres were washed with trichloroethylene (TCE) and NH_4OH and dried in air over night. Hunt and Collins [7] provide an in-depth explanation of the fabrication process.

2.1 Infiltration of dopants into UO_3 spheres

UO_3 microspheres <75 µm, which were fabricated as described above, were dried on a hot plate set at 200 °C. Then, $Mn(NO_3)_2 \cdot 4H_2O$ (Sigma Aldrich) was added to the UO_3 spheres in the respective amounts to aim for 500 ppm and 2,000 ppm Mn in UO_2 (Table 1). Within this report, the dopant concentration is reported as dopant/uranium weight concentration in ppm rather than referring to the oxides. The UO_3 spheres with the $Mn(NO_3)_2 \cdot 4H_2O$ were covered with distilled water, and the manganese nitrate went in solution. The spheres were allowed to absorb the solution for about 7 hours, and the spheres were mixed into the aqueous solution every 30 minutes by hand. The samples were dried under a heat lamp for 1 hour. The following day, the spheres were dried on a hot plate set at 200 °C.

Table 1: Moles of uranium and manganese with the targeted dopant concentration per uranium for the infiltration of the dopant into UO_3 spheres.

ID	n(U) (mmole)	n(Mn) (mmole)	M($Mn(NO_3)_2 \cdot 4H_2O$) (mg)	Mn concentration (ppm) per U
^{530inf}Mn	70.6	0.162	40.6	530
^{2000inf}Mn	69.9	0.606	152.1	2,000

2.2 Addition of dopants to the starting broth

Besides infiltration, a second attempt to add dopants into UO_2 was to directly add the dopants to the starting solutions of the sol-gel experiments. Ideally, a water-soluble composition of the desired dopant was chosen for these experiments.

2.2.1 Addition of Mn to the starting broth

For the addition of manganese, $Mn(NO_3)_2 \cdot 4H_2O$ (Sigma Aldrich) was a suitable composition because manganese nitrate is water soluble. The desired amount (Table 2) of $Mn(NO_3)_2 \cdot 4H_2O$ was added to the ADUN solution, and it dissolved readily. To ensure a homogeneous solution, the bottle was shaken by hand. The ADUN and HMTA/urea solutions were chilled prior to mixing. After mixing, no precipitation of solids was observed, so it was assumed that all $Mn(NO_3)_2 \cdot 4H_2O$ went into a homogeneous solution with the starting broth of the gelation experiment. The gelation experiment was performed using the same process that was used for the nominally pure UO_3 feedstock production, which is described at the beginning of Section 2.

Table 2: Moles of uranium and manganese with the targeted dopant concentration per uranium for the synthesis via addition of the dopant to the starting broth.

ID	n(U) (mmole)	n(Mn) (mmole)	M($Mn(NO_3)_2 \cdot 4H_2O$) (mg)	Mn concentration (ppm) per U
^{190}Mn	83.8	0.0689	17.3	190
^{490}Mn	83.8	0.177	44.4	490
^{510}Mn	318.5	0.706	177.2	510

2.2.2 Addition of Cr to the starting broth

To add chromium oxide as a dopant into the UO_2 spheres, $Cr(NO_3)_3 \cdot 9H_2O$ (Sigma Aldrich) was added in the desired amounts (Table 3) to the HMTA/urea starting solution. The crystals went directly into solution, and the solution was shaken for homogenization. After the HMTA/urea and ADUN solutions were cooled, they were mixed, and no precipitates occurred, indicating that the dopant ($Cr(NO_3)_3 \cdot 9H_2O$) remained in solution. The gelation experiment was conducted using the same process described above for the nominally pure UO_3 feedstock synthesis (Section 2).

Table 3: Moles of uranium and chromium with the targeted dopant concentration per uranium for the synthesis via addition of the dopant to the starting broth.

ID	n(U) (mmole)	n(Cr) (mmole)	M($Cr(NO_3)_3 \cdot 9H_2O$) (mg)	Cr concentration (ppm) per U
^{350}Cr	83.8	0.134	53.8	350
^{780}Cr	82.6	0.294	117.6	780
^{1100}Cr	82.6	0.418	167.2	1,100

3. THERMAL TREATMENT OF FEEDSTOCKS

The as-dried UO_3 spheres were calcined under Ar-4% H_2 atmosphere in a metal tube furnace for 5 hours at 600 ºC to obtain UO_2.

3.1 Thermal treatment of feedstock with dopants

To ensure that the spheres containing dopants were free of any remaining nitrates prior to the calcination step, the spheres were thermally denitrated in air. The individual temperatures and durations for this step were derived by thermogravimetric analysis (TGA) (Section 5.1). UO_3 spheres containing the Mn dopant were thermally denitrated at 350 ºC for 10 hours. UO_3 spheres doped with Cr were thermally denitrated for 10 hours at 500 ºC. The thermal denitration step was followed by a calcination step as described in Section 3.

For the experiment with a concentration of 780 ppm Cr, about half of the spheres showed a green color, whereas the other half showed the anticipated orange color after the thermal denitration step. The green color may be due to an exposure to a higher temperature, or also it may indicate the formation of Cr_2O_3, which has a green appearance. To further investigate the color difference and prove the presence or absence of a secondary Cr_2O_3 phase, Raman or thermogravimetric differential scanning calorimetry (TG-DSC) measurements will be performed in the future. However, the solubility limit of Cr_2O_3 in UO_2 is not thought to be exceeded since the experimental approach targeted for 1,100 ppm Cr, did not show the same behavior. Therefore, the most plausible explanation for the green color seems to be a temperature gradient; this was also observed in previous ceria gelation experiments [8].

4. FABRICATION OF PELLETS

To fabricate UO_2 fuel pellet candidates, the sol-gel microsphere pelletization (SGMP) approach [9][10][11] was applied. Therefore, the calcined UO_2 microsphere feedstock was directly utilized into pellets via cold pressing and sintering [1], for 6 hours at 1,700 ºC in an Ar-4%H_2 atmosphere.

4.1 Reference pellet from UO_2 spheres

Reference pellets of nominally pure UO_2 were fabricated in an earlier study using the calcined UO_2 spheres [1]. Highly porous UO_2 microspheres are favorable for the fabrication of highly dense UO_2 pellets [8]. Porous UO_2 microspheres of different sizes were mixed to achieve efficient packing of microspheres in the pressing die [12]. Therefore, highly favorable starting conditions were achieved to fabricate a highly dense UO_2 pellet.

4.2 Pellets from UO_2-dopant microspheres

The uranium dioxide spheres with a targeted amount of 490 ppm Mn were used to fabricate a UO_2-MnO pellet; 35 mg of each of the calcined sphere size fractions—425–500 µm, 500–600 µm and 1,000–1,180 µm—were mixed and poured into a 4 mm pressing die. The spheres were compacted at 200 MPa for 2 minutes and were sintered as described above (Section 4). The sphere size fractions refer to the sphere sizes of the dried spheres prior to any thermal treatment.

42 mg of each of the size fractions—425–500 µm, 710–850 µm and 850–1,000 µm of the calcined 350 ppm Cr doped UO_2 spheres were mixed and transferred into the 4 mm pressing die. The spheres were compacted into a pellet at 200 MPa for 2 minutes and sintered as described above.

5. CHARACTERIZATION OF FEEDSTOCKS CONTAINING DOPANTS

5.1 Thermal characterization

To identify appropriate temperatures for the thermal denitration step of the as-prepared feedstocks with dopants, TGA was performed. 166 mg of the 2000-Mn-inf feedstock (Table 1) were weighed in an Al_2O_3 crucible and heated in synthetic air in a simultaneous thermal analyzer, 449 F3 Jupiter from Netzsch. The heating rate was 3 °C/min, and the Mn doped sample was heated to 350 °C with a dwell time of 5 hours (Figure 1a). For the analysis of the 350 ppm Cr doped feedstock, 1,757.8 mg of the 425–500 µm spheres were placed in an Al_2O_3 crucible, and the sample was heated in synthetic air at the same heating rate to 500 °C with a dwell time of 10 hours (Figure 1b).

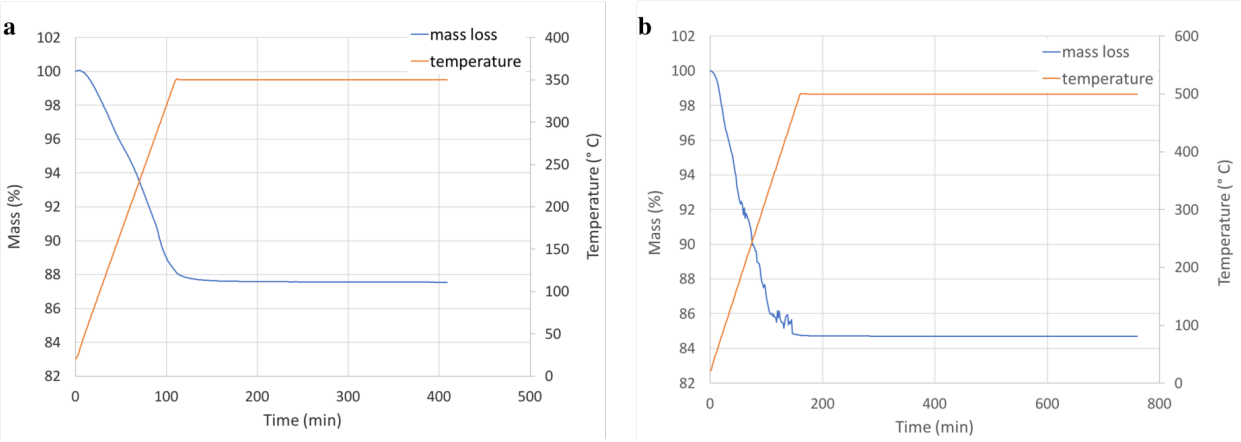

Figure 1: TGA curves in air for the thermal denitration of (a) 2,000 ppm Mn concentration in UO_2 added via infiltration; (b) 350 ppm Cr concentration in UO_2 added to the broth.

The TGA curves in Figure 1a and b confirm the chosen temperatures of 350 °C and 500 °C to be sufficient for removal of nitrate, ammonia, and water residues in the Mn and Cr doped UO_3 spheres, respectively, as no mass change is observed after reaching these temperatures and some dwell time. The temperatures for these thermal treatments prior to calcination were chosen based on literature findings. Gubrynowicz et al. [13] and Malecki et al. [14] studied the thermal decomposition of $Cr(NO_3)_3 \cdot 9H_2O$ in air, and both describe the thermal decomposition to crystalline Cr_2O_3 occurring at a temperature below 500 °C. Regarding $Mn(NO_3)_2 \cdot 4H_2O$, De Bruijn et al. [15] describe the thermal decomposition occurring in two steps, via the formation of a manganese oxonitrate into MnO_2 below 300 °C.

5.2 Density

The slow pour densities were measured of the as-prepared spheres, and for some doped feedstocks, they were measured after the thermal denitration step (Table 4). The spheres were slowly poured into a graduated cylinder, and then the weight and volume of the spheres were determined. All spheres had fairly low slow-pour densities at around 1 g/mL, which is favorable for the direct transformation of the spheres into pellets by cold pressing and subsequent sintering [8].

Table 4: Slow-pour densities of the doped UO_3 microspheres as prepared after drying and after the thermal denitration step.

Sample ID	Slow pour density (g/mL) of as prepared spheres	Slow pour density (g/mL) of thermally denitrated spheres
^{190}Mn	1.08	-
^{490}Mn	0.96	-
^{510}Mn	1.02	1.15
^{350}Cr	1.19	-
^{780}Cr	1.07	1.16
^{1100}Cr	1.13	1.28

To gain insight into the densification of the doped spheres during the thermal treatments, a collection of calcined UO_2 spheres doped with 510 ppm Mn (425–500 µm size fraction) were suspended in oil and imaged by x-ray computed tomography (XCT) using an Xradia MicroXCT-400. Reconstruction of the series of two-dimensional radiographs produced a three-dimensional image of the particles with image brightness corresponding to x-ray absorbance. The initial intent was to digitally segregate the bright uranium oxide particles from each other and the surrounding oil to determine the mean and distribution of the particle volume. However, reconstruction artifacts caused by the high x-ray absorbance of uranium made quantitative segregation unfeasible. This issue may be resolved in future work by reducing the diameter of the particle holder to reduce the impact of reconstruction artifacts. Although quantitative analysis was not achievable with these imaging conditions, the images provide significant qualitative information on the nature of the uranium oxide particles. Figure 2 shows an XCT image of the calcined spheres. Most of the spheres do not show any major porosity, whereas other spheres show fissures rather than enclosed porosity at different locations within a sphere.

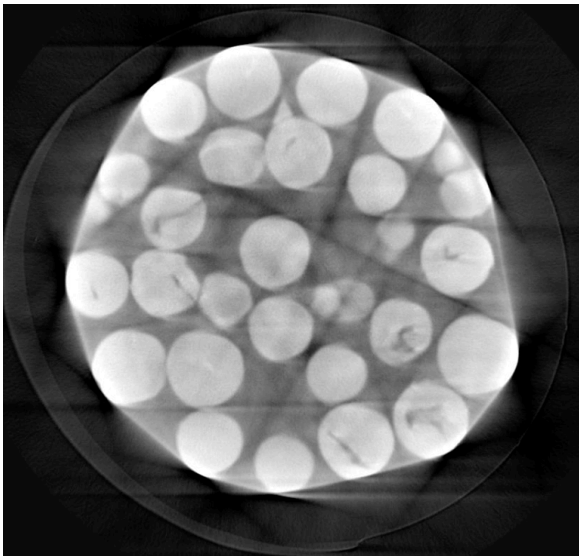

Figure 2: XCT image of the 425–500 µm size fraction of the 510 ppm Mn-doped UO_2 spheres.

The densities of the Mn- and Cr-doped UO_2 pellets were determined geometrically. The 490 ppm Mn-doped UO_2 pellet had a theoretical density (TD) of 96%, and the 350 ppm Cr-doped UO_2 pellet had a TD of 94%. The first efforts to fabricate highly dense pellets using the doped microspherical feedstock were successful for both dopants.

5.3 Structural characterization by x-ray diffraction

After sintering at 1700 °C for 6 hours, the 490 ppm Mn-doped UO_2 spheres were structurally characterized by x-ray diffraction (XRD). Therefore, about 10 mg of the spheres were ground with a mortar and pestle under isopropyl alcohol and prepared on a Si wafer. The sample holder was covered with Kapton foil, encapsulating the radioactive sample to avoid contamination of the instrument. Patterns were collected from 10–110° with a D2 Phaser from Bruker with a Cu k_α source with λ= 1.5406 Å. The XRD pattern in Figure 3 reveals the UO_2 pattern with the fluorite structure. The broad feature at low 2Theta angles was caused by the Kapton foil. No secondary phase could be identified, which indicates a solid solution formation of UO_2 with the dopant. However, the dopant concentration is fairly low, and further characterization techniques confirming the doped UO_2 to be a single phase solid solution are under exploration.

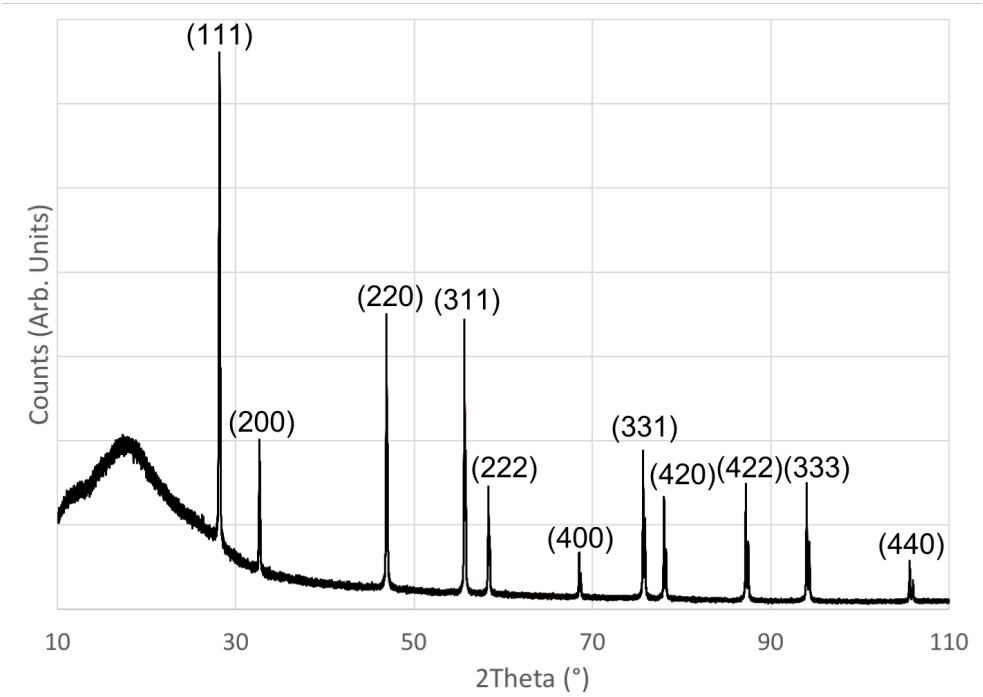

Figure 3: XRD pattern of the 490 Mn-doped UO_2 spheres after heat treatment at 1700 °C for 6 hours.

5.4 Microstructural characterization by scanning electron microscopy

The 490 ppm Mn-doped UO_2 pellet, an individual sphere, and the 350 ppm Cr UO_2 pellet were microstructurally characterized via scanning electron microscopy (SEM). The images were taken with a Phenom XL SEM from Nanoscience Instruments. Figure 4a shows a single sphere after sintering, which consists of multiple grains and remains its spherical shape after sintering. Therefore, the sol formulations chosen in this case were suitable for avoiding cracking spheres during thermal treatments. Figure 4b shows the microstructure of the pellet pressed from the 490 Mn-doped UO_2 spheres. The microstructure shows enlarged UO_2 grains with diameters up to 80 µm, indicating the presence of Mn in the feedstock, to have a positive impact on enlarged grain growth within UO_2 pellets. According to the SEM images, the SGMP approach to fabricate advanced UO_2 fuel candidate pellets presented herein was successful.

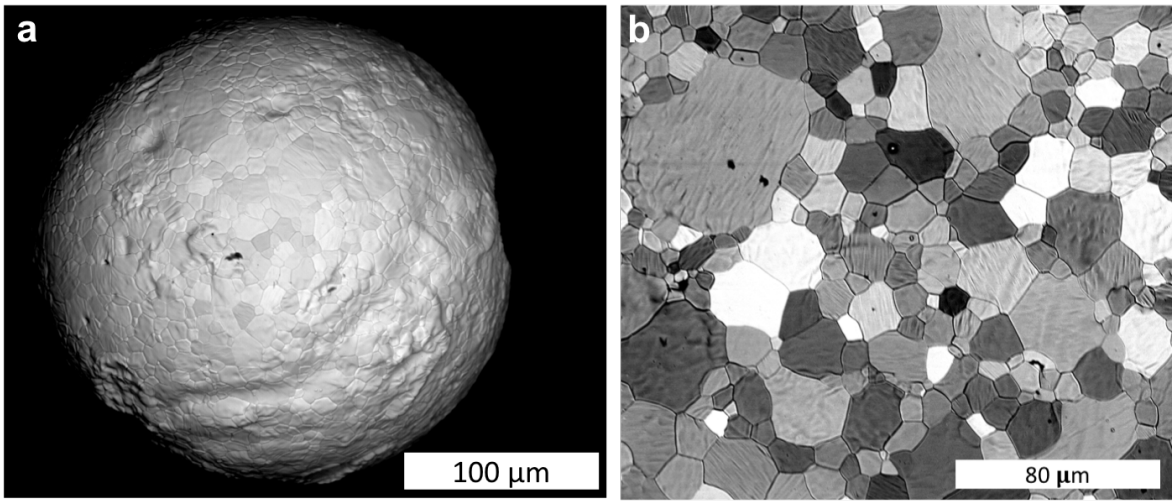

Figure 4: (a) Sintered 490 ppm Mn doped UO_2 sphere after sintering at 1700 °C for 6 hours, (b) 490 ppm Mn doped UO_2 pellet.

The pellet pressed from the 350 ppm Cr-doped spherical feedstock showed enlarged grains (Figure 5), several of which exhibited a diameter > 50 µm. The SEM images of the Mn- and Cr-doped UO_2 pellets indicate enlarged grain growth in UO_2 for pellets fabricated from doped microspherical feedstocks, confirming that the dopant's presence causes enlarged grain growth in UO_2 during sintering.

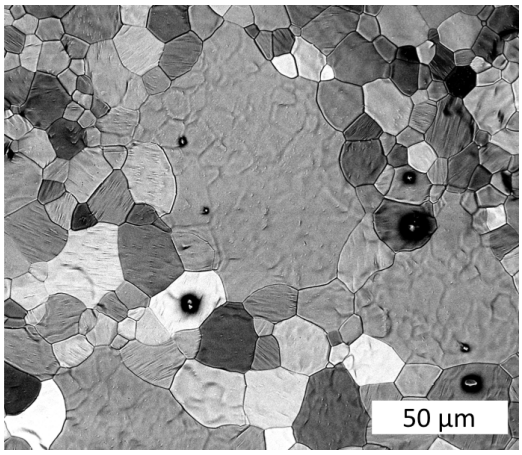

Figure 5: SEM image of the 350 ppm Cr-doped UO_2 pellet after sintering.

5.5 Chemical analysis by inductively coupled plasma mass spectrometry

To probe the actual dopant concentration within the microspherical feedstock, the as-prepared, thermally denitrated, calcined, sintered spheres were analyzed by inductively coupled plasma mass spectrometry (ICP-MS). About 10 mg of each sample were dissolved in 5 mL of 5 M HNO_3 (ultrapure) to bring the spheres into solution. The sintered UO_2 spheres with 350 ppm and 1,100 ppm Cr did not go completely into solution prior to the measurements.

Figure 6a shows the Mn concentrations determined via ICP-MS measurements for the infiltration experiments (Section 2.1). The error for the values was determined by adding the uncertainty of 10% for the detection of the dopant concentration (manganese or chromium) to the uncertainty for the concentration of uranium by ICP-MS (10%). For the experimental approach using ^{530inf}Mn (Table 1), the Mn concentration was determined to be 580 ppm (Figure 6a, blue circle). This value did not change until the sintering step,

confirming that the dopant did not volatize at temperatures up to 600 °C. After sintering for 6 hours at 1700 °C, the dopant concentration dropped below 10 ppm Mn, indicating that the dopant volatized during the sintering step. For the ^{2000inf}Mn experiment (Figure 6a, orange circle), the dopant concentration varies between 2,100–2,250 ppm Mn between the as-prepared and calcined spheres. This is in accordance with the targeted value of 2,000 ppm Mn and is constant within the limit of error for these measurements. After sintering, the Mn concentration dropped to 50 ppm. Figure 6b presents the Mn dopant's concentration for the experimental approaches, where the dopant $Mn(NO_3)_2{\cdot}4H_2O$ was added to the ADUN solution (Table 2) at the beginning of the gelation experiments. For the targeted concentration of 190 ppm Mn, a concentration of 145 ppm Mn was detected, which was constant until after the calcination step (blue circle, Figure 6b). Sintering led once more to a drastic concentration drop to 20 ppm Mn in UO_2. The spheres with a targeted concentration of 490 ppm Mn (orange circle, Figure 6b) varied between 240 ppm and 267 ppm Mn, which is considered to be constant within the limit of uncertainty of the measurement. As observed for the previous spheres, the Mn concentration dropped to 40 ppm Mn after sintering. For the 510 ppm targeted Mn synthesis, a concentration between 260 and 250 ppm Mn (gray circle, Figure 6b) was determined after the thermal denitration and calcination step, respectively. The sintering step the dopant concentration dropping drastically to 30 ppm Mn.

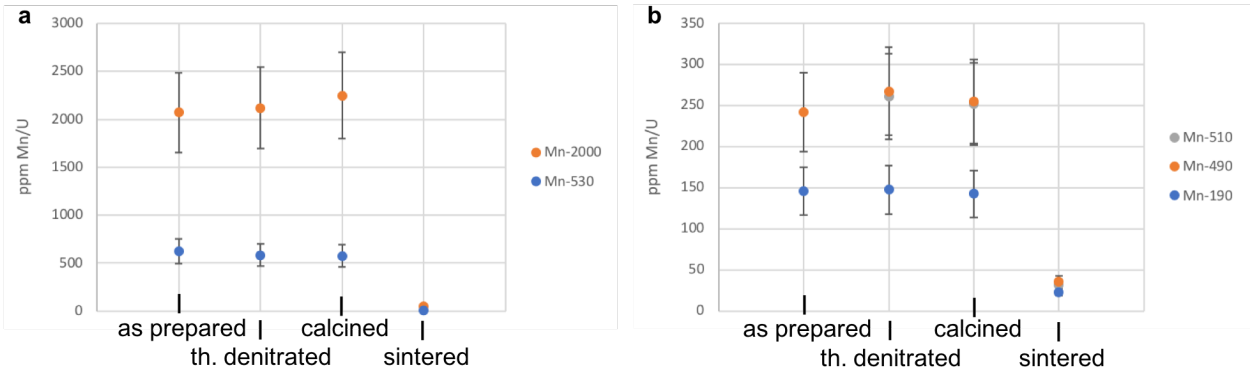

Figure 6: Mn dopant concentration in ppm per uranium—(a) data for the infiltration experiments for a targeted dopant concentration of 530 ppm (blue) and 2,000 ppm (orange) (Table 1), and (b) data for the experiments in which Mn was added to the broth with a targeted Mn concentration of 190 ppm Mn (blue), 490 ppm (orange) and 510 ppm Mn (grey) (Table 2).

Compared to the infiltration experiments (Figure 6a) in which the dopant concentration equals the targeted dopant concentration for all steps prior to sintering, the experiments in which $Mn(NO_3)_2{\cdot}4H_2O$ was added to the ADUN solution (Figure 6b) show a lower dopant concentration than initially targeted, even prior to the sintering step. However, the dopant concentration does not change during the thermal denitration and calcination, but it is already lower in the as dried spheres than expected. This is even more pronounced for the higher dopant concentrations of 490 and 510 ppm when compared to the 190 ppm Mn experiment. A possible explanation could be the formation of $Mn(OH)_2$ during the gelation experiment, which is soluble in alkaline conditions. The ammonia washes after the gelation of the droplets could therefore lead to a partial washing out of the manganese by a partial solution of $Mn(OH)_2$. However, this is only a hypothesis at this stage and will require further experimental investigation and evidence. Since the infiltered spheres do not undergo any further washing steps with ammonia, this could also explain the detected Mn concentration meeting the targeted concentration. The sintering step led to a drastic decrease of the Mn concentration for both of the experimental approaches, indicating that the dopant volatized during the thermal treatments at higher temperatures, independent of the experimental approach to include the dopant within the UO_3 microspherical feedstock.

Figure 7 shows the Cr concentration for the experiments in which Cr was added to the HMTA/urea solution at the beginning of the sol-gel synthesis (Table 3). The experiment targeted for 350 ppm Cr (blue circle, Figure 7) showed a Cr content of 360–380 ppm Cr for the spheres prior to sintering, which confirmed the

targeted concentration. Sintering led to a drastic drop of the dopant concentration to 85 ppm Cr. For the 780 ppm Cr-targeted experiments, the Cr concentrations for the green (green circle, Figure 7) and orange spheres (orange circle, Figure 7) are within the uncertainty of the measurement, and this result is the same after thermal denitration as well as calcination. The sintered spheres of both colors show a strong decrease in the Cr concentration. However, along with the remaining 400 ppm Cr the green spheres contain more than two and a half times more Cr than the orange spheres, in which only 150 ppm Cr remain within the spheres. This indicates that there are different chemical compositions for spheres of different colors. For the 1,100 ppm Cr-targeted experiment (Figure 7, yellow circle), the measured concentration of Cr was 1,060 ppm, and this did not change until the sintering step, where it dropped to 340 ppm. Compared to the experiments in which $Mn(NO_3)_2 \cdot 4H_2O$ was added to the starting broth of the gelation experiment and a lower dopant concentration than targeted was observed from the ICP-MS measurements, the experiments with $Cr(NO_3)_3 \cdot 9H_2O$ show the synthesized UO_3/UO_2 spheres to contain the targeted dopant concentration after each step of the thermal treatment prior to sintering.

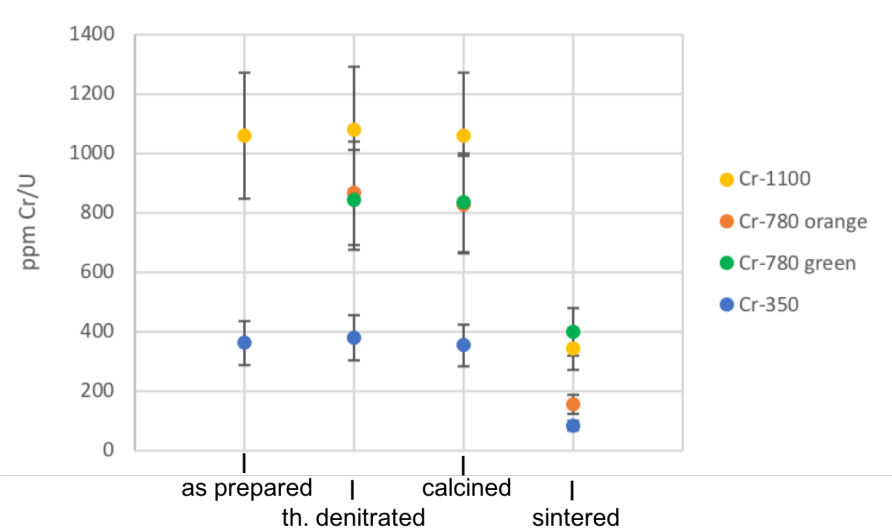

Figure 7: Cr dopant concentration in ppm per uranium for experiments in which Cr was added to the broth with a targeted Cr concentration of 350 ppm Cr (blue), 780 ppm (green & orange) and 1,100 ppm Cr (yellow) (Table 3).

ICP-MS of the sintered spheres showed a rather drastic loss of the dopant for all experimental approaches, as well as dopants and concentrations. To gain insight regarding the temperatures at which the dopants volatize, a systematic study of the sintering temperature is planned, starting at lower temperatures, and other options such as hot pressing may be explored.

6. CONCLUSIONS AND OUTLOOK

The addition of Mn and Cr as dopants to UO_2 is expected to promote grain growth within UO_2 pellets [2]. The objective of this study was to develop a fabrication route to synthesize a feedstock containing controlled dopant amounts. It was demonstrated in earlier work that a microspherical feedstock is a highly suitable precursor for pellet fabrication [1]. In particular, the absence of dust formation in the case of the SGMP approach—in which the microspheres are directly used to prepare a pellet via cold pressing and a subsequent sintering step—make it a superior approach as compared to conventional powder processing routes. Moreover, the internal gelation approach is highly flexible, allowing for (1) dopants to be included to form a solid solution with the main phase, or (2) a secondary phase to be added to the main phase of the microspheres. This flexibility is favorable for more the complex precursor formulations, as aimed for within this study. The infiltration of manganese into UO_3 spheres led to the targeted uptake of the dopant, which did not alter until the sintering step. The addition of manganese to the UO_2 spheres via addition of $Mn(NO_3)_2 \cdot 4H_2O$ to the starting broth of the gelation experiments led to lower Mn concentrations than targeted. This may be due to some $Mn(OH)_2$ going into solution during the washing steps with NH_4OH. Further experimental investigations must be undertaken to confirm this theory. The synthesis of a microspherical UO_3 feedstock with controlled Cr dopant concentrations ranging from 350–1,100 ppm by addition of $Cr(NO_3)_3 \cdot 9H_2O$ to the HMTA/urea's starting broth resulted in the uptake of the targeted Cr concentrations within the microspheres. The dopant concentration dropped drastically in all sintered microspheres, but the loss of dopant was more pronounced for the Mn-doped UO_2 spheres. First approaches to fabricate dense pellets with the here fabricated feedstock led to highly dense doped UO_2 pellets, with 94% and 96% TD for Cr and Mn doped pellets, respectively. Regardless of the concentration drop of the dopants in the sintered spheres, SEM images of the pellets fabricated from Cr- or Mn-doped spheres led to much larger UO_2 grains of up to 80 µm within the fuel candidate pellets as compared to UO_2 grains in nominally pure UO_2 pellets. However, the decrease of the dopant concentration during sintering is not surprising, because Kashibe and Une [4] already observed a drastic drop in the dopant concentration for Cr of 47% in UO_2 during the sintering step.

Future work will focus on identifying the temperature at which the dopant loss occurs and will explore possible alternate routes for pellet processing, e.g., by hot pressing. Additionally, the confirmation of a solid solution formation of the dopants with the UO_2 within the feedstock will be studied in the future. Neutron diffraction experiments are planned to further investigate the structural changes caused by the aliovalent dopants, which most likely will result in changes in the oxygen sublattice. Moreover, pellets of different dopant concentrations will be prepared to study the in-reactor performance via irradiation experiments at ORNL's High Flux Isotope Reactor (HFIR) within the MiniFuel irradiation setup.

7. References

[1] S. C. Finkeldei, J. Kiggans, R. D. Hunt, K. A. Terrani, A. T. Nelson, Fabrication and microstructural analysis of ceramic fuel derived from sol-gel and powder routes, Oak Ridge, 2018. ORNL/SPR-2018/866 Revision 1.

[2] M. W. D. Cooper, C. R. Stanek, and D. A. Andersson, The role of dopant charge state on defect chemistry and grain growth of doped UO_2, Acta Mater. 150 (2018) 403–413. doi:https://doi.org/10.1016/j.actamat.2018.02.020.

[3] A. R. Massih, Effects of Additives on Uranium Dioxide Fuel Behavior, 2014. Report number:2014:21, ISSN:2000-0456.

[4] S. Kashibe, K. Une, Effect of additives (Cr_2O_3, Al_2O_3, SiO_2, MgO) on diffusional release of ^{133}Xe from UO_2 fuels, J. Nucl. Mater. 254 (1998) 234–242. doi:https://doi.org/10.1016/S0022-3115(97)00356-5.

[5] J. Arborelius, K. Backman, L. Hallstadius, M. Limbaeck, J. Nilsson, B. Rebensdorf, G. Zhou, K. Kitano, R. Loefstroem, G. Roennberg, Advanced Doped UO_2 Pellets in LWR Applications, J. Nucl. Sci. Technol. 43 (2006) 967–976.

[6] K. W. Kang, J. H. Yang, J. H. Kim, Y. W. Rhee, D. J. Kim, K. S. Kim, K. W. Song, Effects of MnO-Al_2O_3 on the Grain Growth and High-Temperature Deformation Strain of UO_2 Fuel Pellets, J. Nucl. Sci. Technol. 47 (2010) 304–307. doi:10.1080/18811248.2010.9711958.

[7] R. D. Hunt, J. L. Collins, Uranium kernel formation via internal gelation, Radiochim. Acta. 92 (2004) 909. doi:10.1524/ract.92.12.909.55110.

[8] R. D. Hunt, J. L. Collins, M. H. Lloyd, S. C. Finkeldei, Production of more ideal uranium trioxide microspheres for the sol-gel microsphere pelletization process without the use of carbon, J. Nucl. Mater. 515 (2019) 107–110.

[9] E. Zimmer, C. Ganguly, J. Borchardt, H. Langen, SGMP — an advanced method for fabrication of UO_2 and mox fuel pellets, J. Nucl. Mater. 152 (1988) 169–177. doi:https://doi.org/10.1016/0022-3115(88)90323-6.

[10] S. M. Tiegs, P. A. Haas, R. D. Spence, The Sphere-Cal Process: Fabrication of Fuel Pellets from Gel Microspheres, Oak Ridge, 1979. doi:ORNL/TM-6906.

[11] R. B. Matthews, P.E. Hart, Nuclear fuel pellets fabricated from gel-derived microspheres, J. Nucl. Mater. 92 (1980) 207–216. doi:https://doi.org/10.1016/0022-3115(80)90104-X.

[12] J. E. Ayer, F. E. Soppet, Vibratory Compaction: I, Compaction of Spherical Shapes, J. Am. Ceram. Soc. 48 (2006) 180–183. doi:doi:10.1111/j.1151-2916.1965.tb14708.x.

[13] L. Gubrynowicz, T. Strömich, Study on the thermal decomposition of chromium(III) nitrate nonahydrate (CNN), Thermochim. Acta. 115 (1987) 137–151. doi:https://doi.org/10.1016/0040-

6031(87)88360-0.

[14] A. Małecki, B. Małecka, R. Gajerski, S. Łabuś, Thermal decomposition of chromium(III) nitrate(V) nanohydrate, J. Therm. Anal. Calorim. 72 (2003) 135–144. doi:10.1023/A:1023915618876.

[15] T. J. W. De Bruijn, G. M. J. De Ruiter, W. A. De Jong, P. J. Van Den Berg, Thermal decomposition of aqueous manganese nitrate solutions and anhydrous manganese nitrate. Part 1. Mechanism, Thermochim. Acta. 45 (1981) 265–278. doi:https://doi.org/10.1016/0040-6031(81)85087-3.